Pergamon

Planet. Space Sci., Vol. 45, No. 5, pp. 585–593, 1997

0032-0633/97 $17.00+0.00

PII: S0032-0633(97)00029-9

Visual observations of the Perseid meteor shower 1988–1994

Jürgen Rendtel[1] **and Peter Brown**[1,2]

[1]International Meteor Organization, PF 60 01 18, D-14401 Potsdam, Germany
[2]Department of Physics and Astronomy, University of Western Ontario, London, Ont., Canada N6A 3K7

Received 2 September 1996; accepted 20 January 1997

Abstract. Visual meteor observations are used to determine the flux profile of the Perseid stream from 1988 to 1994. The position and peak flux of recently detected outburst maxima are found for each year as is the location and magnitude of the regular maximum. The Perseid stream is found to consist of three primary components; a long-lived and relatively weak background component, a core component which is active for 1–2 days near the main peak of the shower and an outburst component which is active for only a few hours. The outburst peaks show a systematic variation in terms of the solar longitudes of the peak. The position of the outburst shifted backwards in solar longitude (J2000.0) from $\lambda_\odot = 139°.78$ in 1988 to $\lambda_\odot = 139°.48$ in 1992, when it occurred closest to the node of 109P/Swift-Tuttle (139°.44). In subsequent years the peak position shifted forward again to $\lambda_\odot = 139°.59$ in 1994. The magnitude of the peak flux shows a significant difference between returns before 1991 as compared to those after this year. This may indicate an ejection origin other than 1862 for outburst material encountered before 1991. The particle composition of the outburst maximum and core maximum are indistinguishable. A double maximum in the population index associated with these activity maxima has been detected in the average Perseid profile. High temporal resolution study of the flux profile of the ascending branches of the outburst profiles in 1993 and 1994 suggest that this component may consist of sub-components, possibly of differing ages. © 1997 Elsevier Science Ltd

1. Introduction

The Perseid meteor shower is among the strongest and best observed meteor showers currently visible on Earth. According to Hasegawa (1993), the Perseids may have been chronicled for almost two millennia. A detailed historical review of the stream has been given by Kronk (1988).

Interest in the Perseids increased during the late 1970s in anticipation of the return of 109P/Swift–Tuttle, which was expected to reach perihelion *c.* 1980 (Marsden, 1973). The comet, however, was not recovered within this time period. In 1988 and 1989 a new peak located some 12 h before the regular Perseid maximum and of similar strength to the regular maximum was detected (Roggemans, 1989; Koschack and Roggemans, 1991). This new peak represented early detection of new meteoroids associated with the impending return of 109P/Swift–Tuttle. The position of the new activity peak in these years was very close to the nodal longitude of the comet ($\lambda_\odot = 139°.44$, J2000.0) which was recovered in September 1992 (Marsden *et al.*, 1993; Yau *et al.*, 1994). Subsequently, stronger outbursts in activity were recorded from the Perseids between 1991 and 1994. This outburst component has been observed as late as 1996 (Rendtel and Arlt, 1996).

Here we present results obtained from visual meteor observations of the Perseids near its time of maximum for the years 1988–1994. In total 14,552 count intervals were used for this study. This represents data collected by 1115 observers from 38 countries who reported 243,227 Perseid meteors during 14,237 h of effective observational time.

The method used to observe meteors and reduce these data follows from the development of the visual techniques summarized by Kresáková (1966). All data are based on reports of individual observers, giving the number of meteors seen (Perseids, non-Perseids), the stellar limiting magnitude LM, the effective observing time T_{eff} and the cloud cover as well as the geographic coordinates of the observing site. The data are stored in the Visual Meteor DataBase (VMDB) of the International Meteor Organization (IMO). The analysing method actually applied is shortly summarized by Brown and Rendtel (1996) and outlined by Koschack and Hawkes (1995) and

Correspondence to: J. Rendtel

Koschack (1995). The complete reduction techniques for visual observations have been developed and discussed by Koschack and Rendtel (1988, 1990a, b).

First, the magnitude data are used to determine the population index r as a function of solar longitude. The population index gives the slope of the cumulative magnitude function of the shower meteors. Since the probabilities of perception become uncertain towards fainter meteor magnitudes, we restrict the analysis to meteors 2 mag brighter than the limiting magnitude LM (Koschack, 1995). Using this profile of r, we calculated the Zenithal Hourly Rate (ZHR; i.e. the number of meteors from a shower a standard observer would see under unobstructed skies with the radiant point overhead and LM = 6.5) from each observation interval. The ZHR is defined as

$$\mathrm{ZHR} = \frac{N r^{6.5-\mathrm{LM}}}{\sin^{\gamma}(H_{\mathrm{rad}}) T_{\mathrm{eff}}}. \quad (1)$$

Here N is the number of shower meteors observed during the effective observing time T_{eff} with the radiant altitude being H_{rad} at the middle of the interval. We applied an exponent $\gamma = 1$, as discussed in Brown and Rendtel (1996).

The selection criteria applied to all data in this study required that:

- The altitude of the Perseid radiant was greater than 20° during the observation interval.
- The total correction factor (the value multiplying N in equation (1)) was less than 5.
- The LM > 5.5, with the exception of Perseid returns where the Moon was present.

The individual ZHRs are then averaged over time intervals. *Systematic* deviations from the average by each observer are used to determine a perception correction for each observer (Koschack and Rendtel, 1990b). The ZHR curve is then recalculated using these individual perception coefficients. A final ZHR curve is computed based on a sliding-average over short-time intervals whose minimum size depends on the duration of the individual counting intervals.

With the profiles of r and the ZHR computed, the spatial number density S in the stream can be determined using the procedures described by Koschack and Rendtel (1990a, b). The values for S are given in units of meteoroids per 10^9 km^3.

For the profiles of S, the formal errors represent the standard deviations of the set of observations where all errors are taken to be uniformly random and the resulting distributions are assumed to be Gaussian. Effects of systematic errors are more difficult to establish, but data strongly affected in this way are detected through examination of secondary criteria (such as the sporadic rate) and removed from further analysis.

The values of the number density S strongly depend on the population index r. Hence features found in the ZHR profile may appear amplified or attenuated in the corresponding profile of S for (local) high or low values of r, respectively. The r profiles are based on smaller samples than the ZHR profiles, and the individual numerical values for r depend on the probabilities of perception which have been determined only for a few observers (Koschack and Rendtel, 1990a). We therefore refer to local maxima obtained from the ZHR figures (Brown and Rendtel, 1996).

2. Results of Perseid observations 1988–1994

The shape of the spatial number density profiles S shown in Figs 1–7 are generally similar, though significant vari-

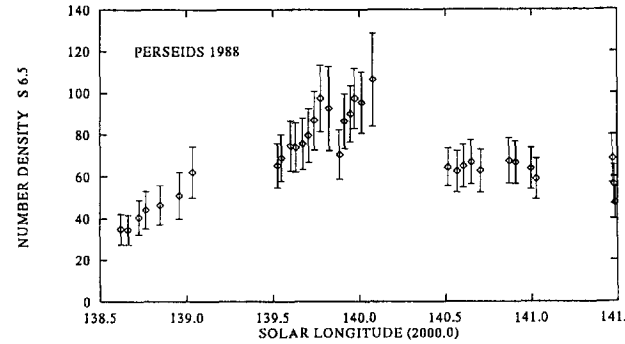

Fig. 1. The spatial number density ($S_{6.5\,\max}$) for the 1988 Perseid return. The data are well distributed about both maxima. This was the first year that the "new" maximum was detected, in this case at $\lambda_\odot = 139°.78$, about 6 h before the traditional peak which took place at $\lambda_\odot = 140°.08$ (Roggemans, 1989). The old and new maxima were of very similar activity, but there are insufficient magnitude data to determine if the particle composition differed between the peaks. The ascending branch of the early maximum is well defined and shows a half-width-to-half-maximum (HWHM) activity above the general profile of 1 h. The descending branch is not well defined, but the few data here suggest a similar decline to a local minimum before activity again increases to the normal maximum. The descending branch of the main maximum is missing in these data and a higher maximum than shown here is possible, though the data do cover the interval during which the normal Perseid peak traditionally occurs and where it is well covered in later data

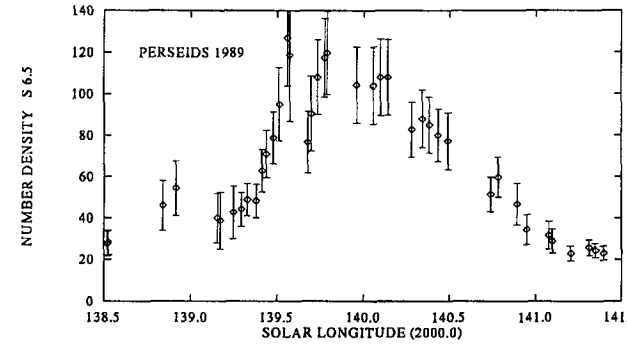

Fig. 2. The spatial number density ($S_{6.5\,\max}$) for the 1989 Perseid return. The profiles shown here are similar to 1988 for times away from the maxima. The early maximum occurs at $\lambda_\odot = 139°.56$ while the normal maximum is at $\lambda_\odot = 139°.8$. The magnitude of the maxima are again similar. The ascending branch of the early peak has a HWHM of 2 h and is well defined. The descending branch from the early peak is not documented in 1989 due to uneven observer coverage. The rising portion of the main profile shows a clear peak followed by several closely spaced points of decline, suggesting the maximum is better located than in 1988. Several features are notable in the falling portion of the main maxima, namely at $\lambda_\odot = 140°.1$ and 140°.3

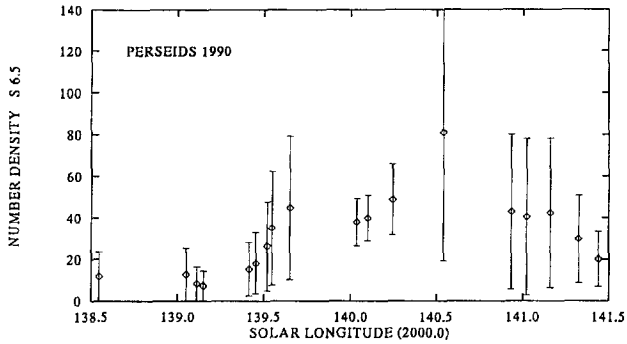

Fig. 3. The spatial number density ($S_{6.5\,max}$) for the 1990 Perseid return. Data are heavily contaminated by the Moon which was full on August 6, 1990 and thus affected all observations during the peak. There appears to be a first peak near $\lambda_\odot = 139°.6$ and a later peak occurring near $\lambda_\odot = 140°.5$ of comparable strength. Neither peak is defined by more than one or two low-weight data points. The low observed rates at peak are likely artifacts of the lunar conditions. Additional error is apparent from the shape of the sporadic activity curve which closely mimicks the Perseid curve, suggestive of numerous Perseids being counted as sporadic

ations in the population index r, particularly after the main maximum, does tend to broaden the main peak in S. The spatial number density curves shown here are for meteors with a limiting absolute magnitude of 6.5, or equivalent limiting mass of 2×10^{-5} g using the mass–magnitude–velocity relation of Verniani (1973) for normally incident meteoroids.

For the outburst portions of the profile, fainter meteors will tend to be under-represented as observers become overloaded recording meteors. This saturation effect was found by Koschack *et al.* (1993) in a prior Perseid analysis. Hence the values of S shown here for the new peaks are lower limits.

To determine if any structure is present in the outburst component of the stream, the data for 1993 and 1994 near the locations of the outburst are analysed at higher temporal resolutions. Small-scale variations in flux pro-

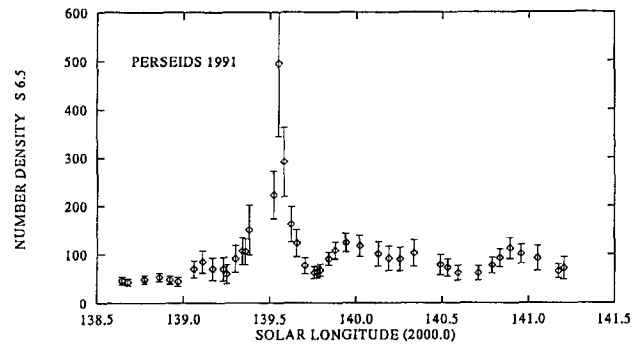

Fig. 4. The spatial number density ($S_{6.5\,max}$) for the 1991 Perseid return. The early peak becomes dominant. The peak times for the maxima are clearly resolved as $\lambda_\odot = 139°.55$ and $139°.94$, respectively. The ascending branch of the early peak has few data, but the HWHM can be roughly estimated as 0.5 h. The descending portions have good coverage and reveal a HWHM of only 1 h. The normal peak shows good coverage in 1991 displaying a HWHM value of 12 h for the descending branch, the ascending branch value being uncertain due to contamination from the earlier peak. There is also an apparent difference in particle makeup since we find a local minimum for r between the early and main maximum

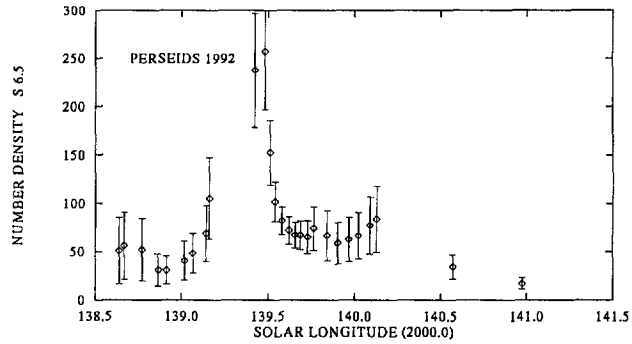

Fig. 5. The spatial number density ($S_{6.5\,max}$) for the 1992 Perseid return. The lunar conditions were poor at the peak, with full Moon occurring on August 13. Nevertheless, good data coverage enabled better determination of the time of peak and its magnitude than in 1990. Information is obtainable about the descending portion of the early peak which was approximately 1 h HWHM and occurred at $\lambda_\odot = 139°.48$. The main maximum appears at approximately $\lambda_\odot = 140°.13$

files near the time of outbursts have been reported in the past associated, e.g. with the Draconids (Lovell, 1954, p. 330) and α-Monocerotids (Rendtel *et al.*, 1996). Here all count intervals greater than 0.5 h were rejected to obtain a high resolution profile with steps as short as $0°.004$ in solar longitude in the immediate region near the outburst peak. The results are shown in Fig. 8a and b where further details are given. Note that 1993 Perseid data are more plentiful than in 1994 by an order of magnitude.

The build up to maximum in 1993 is extremely well defined and may be regarded as consisting of two main components: a gradually increasing branch beginning at $\lambda_\odot = 139°.35$ and continuing to $\lambda_\odot = 139°.49$. In this interval, the slope of the Spatial Number Density–Solar Longitude curve is +7.5 meteoroids per $0°.01$ of solar longitude brighter than +6.5 (hereafter $(M_v > 6.5)$ $0°.01^{-1}$). In the interval from $139°.49$ to $139°.53$ the slope changes dramatically to +43 $(M_v > 6.5)$ $0°.01^{-1}$. These two sections suggest that the outburst component may

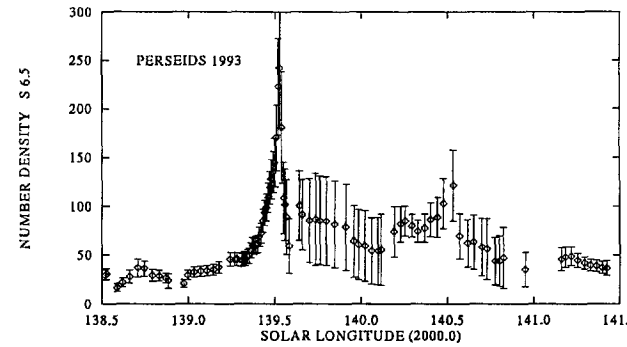

Fig. 6. The spatial number density ($S_{6.5\,max}$) for the 1993 Perseid return. Best coverage of the shower's activity of all years. The profiles in the ascending branch of the early peak is the clearest of any of the profiles, displaying a HWHM of 1.5 h. The descending branch is not well delineated, but the data does suggest that the HWHM for the ascending branch was almost twice as wide as for the descending branch with the early peak occurring at $\lambda_\odot = 139°.53$. The main ZHR maximum was broad in extent, occurring near $\lambda_\odot = 139°.9$. It is not prominent in the number density profile because of a very low value of $r = 1.84$ at this position. Vice versa, the maximum of S at $140°.5$ may be only caused by a single (high) value of $r = 2.3$ at this position

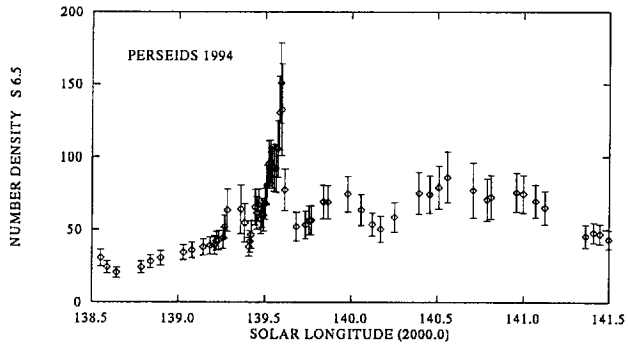

Fig. 7. The spatial number density ($S_{6.5\,max}$) for the 1994 Perseid return. Both, good observer coverage and excellent lunar conditions converged. The ascending portion of the profile is well established with the early maximum occurring at $\lambda_\odot = 139°.59$ and displaying a HWHM of only 1 h. The magnitude data are particularly well defined in 1994 and show a decrease in r after the early peak. A strong asymmetry is present in the population index before and during maximum as compared to after both peaks, when its value gets much larger. The main peak occurs near $\lambda_\odot = 139°.9$, but is difficult to locate precisely due to its broad outline. There is another clear feature in the descending portion of the profile near $\lambda_\odot = 140°.3$ as well as at $\lambda_\odot = 140°.5$

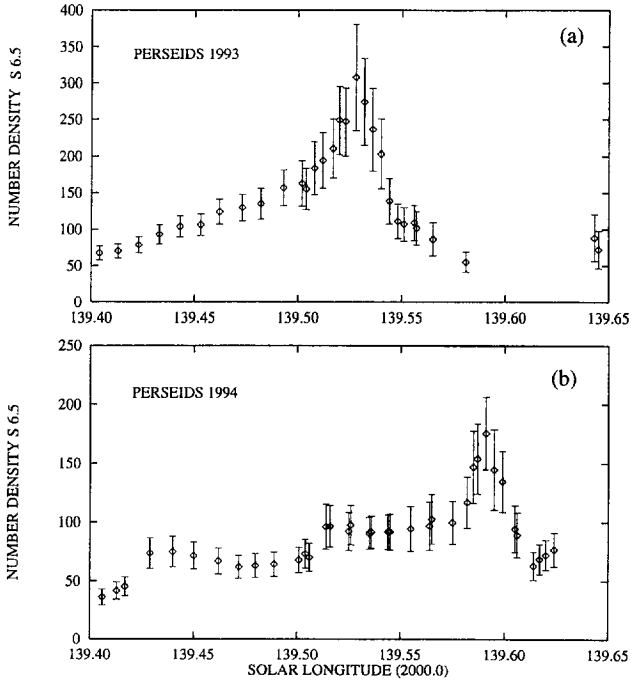

Fig. 8. The spatial number density ($S_{6.5\,max}$) for the 1993 Perseid return at higher temporal resolution (a). In total 1260 individual count intervals were available that were shorter than 0.3 h in length during the central interval and 0.6 h duration in the outer intervals. Between $\lambda_\odot = 139°.30$ and 139°.50 the sampling interval was 0°.02 in length and shifted by 0°.01. From 139°.50 to 139°.56 the sampling interval was 0°.008 in length and was shifted by 0°.004. From 139°.56 to 139°.70 the sampling interval was 0°.02 in length, shifted by 0°.01. The ZHR and spatial number density ($S_{6.5\,max}$) for the 1994 Perseid return at higher temporal resolution (b). In total 124 individual count intervals were available that were shorter than 0.3 h in length during the central interval and 0.5 h duration in the outer intervals. Between $\lambda_\odot = 139°.30$ and 139°.50 the sampling interval was 0°.02 in length and shifted by 0°.01. From 139°.50 to 139°.62 the sampling interval was 0°.008 in length and was shifted by 0°.004. From 139°.62 to 139°.70 the sampling interval was 0°.02 in length, shifted by 0°.01

itself consist of several sub-components of differing ages, the steep increase being associated with the most recent ejecta and the broader increase just before it due to material diffused somewhat from slightly older passages of 109P/Swift–Tuttle. Since the nodal longitude of the comet has been gradually increasing over time, one expects the oldest ejecta to be preferentially before the current nodal longitude of the comet.

The profiles in both the ascending and descending portions of the outburst in 1993 are remarkably smooth. Hints of slight step-like increases of the ZHR near 139°.45 and 139°.39 are present. Due to the larger error bars introduced by the r profile, this variation is masked in the profile of S shown in Fig. 8a. Similar structure is also visible in the 1994 profiles near 139°.43 and 139°.51. The first of these are in an almost identical location in 1993 and 1994 which is extremely close to the current nodal longitude of 109P/Swift–Tuttle. The latter fluctuation in 1994 corresponds closely to the location of maximum in 1993 and suggests that many of the meteoroids associated with the outburst maxima have a small spread in semi-major axis amounting to only a few tenths of an AU or are perturbed into Earth-intersecting orbits effectively for intervals of the order of a year.

In 1994, the outburst profile has fewer data and is less well defined. The build-up to the outburst peak is much slower than in 1993 showing a plateau in activity with a "jump" in activity near 139°.51. The slope of the steeper rising ascending section of the outburst from 139°.57 to 139°.59 is +50 ($M_v > 6.5$) $0°.01^{-1}$; very similar to the slope found in 1993.

3. Discussion

The Perseid stream as described from the visual observations presented here can be broadly delineated into three major components:

- a broad plateau displaying weak activity (background Perseids);
- a more concentrated component centred about the traditional Perseid peak (core Perseids); and
- a strongly time-varying component of short duration which appears in all profiles shortly after the nodal longitude of the parent comet (outburst Perseids).

In order to see the first two components which have only modest variations from year to year, we have synthesized a mean Perseid profile from all available visual observations 1988–1994, excluding intervals which obviously contain the outburst component (Fig. 9). Since the outburst component occurred at varying positions (Table 2), we also got some non-outburst data for the period $\lambda_\odot = 139°.3$–139°.8. Nevertheless, a portion of the outburst component may have been included in the sample.

The *background component* is long-lived and shows weak activity extending from late July ($\approx 115°$) until the end of August ($\approx 150°$). This portion of the Perseid stream shows a very gradual increase in activity until $\approx 138°$ when the activity profile steepens as the core portion of the stream is encountered. The *core component* rises to a peak whose long-term position is $\lambda_\odot = 139°.96 \pm 0°.05$. The steepest section of the peak associated with the core Per-

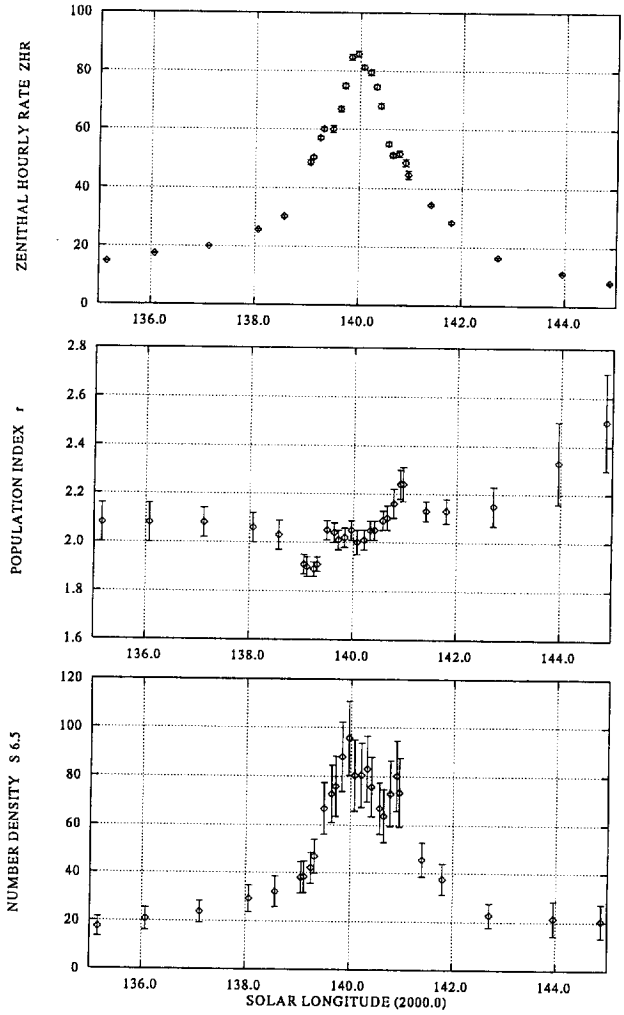

Fig. 9. The ZHR, r and spatial number density ($S_{6.5\,max}$) for the mean Perseid activity in the period 1988–1994 for the full duration of significant activity for the shower

seids is very symmetrical, the ascending portion having a HWHM of $1^\circ.06 \pm 0^\circ.07$ compared to the descending HWHM of $1^\circ.04 \pm 0^\circ.07$. The slight asymmetry in the overall shape of the ZHR curve is most evident at the 1/4-width points, located $2^\circ.58 \pm 0^\circ.07$ before maximum and $2^\circ.35 + 0^\circ.07$ after maximum. From these results, the Perseid shower is above the sporadic background from $\approx 136^\circ$ to 143°.

The average Perseid profile is a superposition of two components and is asymmetrical as shown by Ahnert-Rohlfs (1952), Lindblad (1986), Mason and Sharp (1981), Zvolánková (1984) from visual data and Šimek and McIntosh (1986), Lindblad and Šimek (1986) and Šimek (1987) from radar data.

Harris *et al.* (1995) have modelled the overall activity of the stream through decay of 109P/Swift–Tuttle over a 160,000 year time period. Their model reproduces the asymmetry in the core portion of the stream and also predicts several strong secondary maxima before the main peak, most notably one lasting several days at $\lambda_\odot = 125^\circ$. Such secondary maxima are not present in the mean profile presented here. One explanation for this is that the role of planetary perturbations on stream meteoroids is significant over very long timescales, even for high inclination streams such as the Perseids, the Harris model having ignored such perturbations.

Little structure is evident in the mean ZHR with the possible exception of a maximum near $\lambda_\odot = 140^\circ.9$ and a slight maximum at $\lambda_\odot = 139^\circ.5$, the latter undoubtedly related to the outburst component of the stream which has not been entirely rejected from these data. This may also be a reason for the variations in the profile of r. In addition to these local features, a broad plateau of flux is clearly visible in the spatial number density profile immediately following the main maximum. This is a consequence of the increase in r after the main maximum.

The lack of strong sub-maxima is an expected result, as the smoothing procedures tend to smear-out variations in activity, such sub-maxima being visible primarily in the yearly profiles. Stable sub-maxima in long-term profiles have been noted previously, particularly in radar data on the stream. Table 1 summarizes the reported locations of past sub-maxima detailed in the literature as well as the main maximum.

The most convincing candidates for sub-maxima in these years are located in the region $\lambda_\odot = 140^\circ.2$–$140^\circ.3$. That sub-maxima are present in some years appears probable given the high statistical weight of the visual reports in the present study, but stability of such structures over many years is still questionable based on our results. Such structures may be linked with mean motion resonances operating in the Perseid stream as has been suggested by

Table 1. Locations of the main maximum and reported sub-maxima from recent radar and visual data. $\lambda_\odot$ is the position of the main maximum and $\lambda_{\odot sub}$ the position of any additional sub-maxima. Possible sub-maxima of the ZHR from this work are also given; those values which are less certain are shown in parentheses

Year(s)	$\lambda_\odot$	$\lambda_{\odot sub}$	Source
1980	$139^\circ.92 \pm 0^\circ.04$		Mason and Sharp (1981)
1958–1962, 1972, 1980–1985	$139^\circ.89 \pm 0^\circ.035$	$139^\circ.0$, $139^\circ.5$, $140^\circ.5$, $142^\circ.0$	Šimek (1987)
1958–1964	$139^\circ.91 \pm 0^\circ.026$	$140^\circ.5$	Šimek and McIntosh (1986)
1953–1978	$139^\circ.90 \pm 0^\circ.035$	$140^\circ.46$	Lindblad and Šimek (1986)
1953–1981	$140^\circ.11$	$140^\circ.45$	Lindblad (1986)
1964–1981	$139^\circ.7 \pm 0^\circ.2$		Andreev *et al.* (1987)
1989	$139^\circ.80 \pm 0^\circ.09$	$140^\circ.1$, $140^\circ.3$, ($140^\circ.9$)	This work
1991	$139^\circ.94 \pm 0^\circ.04$	($140^\circ.34$), $140^\circ.9$	This work
1993	$139^\circ.91 \pm 0^\circ.04$	$140^\circ.2$, ($140^\circ.5$)	This work
1994	$139^\circ.84 \pm 0^\circ.04$	$140^\circ.3$, ($140^\circ.5$)	This work

Table 2. The locations and magnitude of the Perseid maxima from 1988 to 1994. $\lambda_{\odot 1}$ is the position of the first (new) maximum and $\lambda_{\odot 2}$ the position of the second (normal) maximum. Both locations refer to the ZHR maxima. The spatial number densities associated with the first peak ($S_{6.5\,\text{outburst}}$) and the second maximum ($S_{6.5\,\text{max}}$) are also given in units of meteoroids brighter than abolute magnitude +6.5 per $10^9\,\text{km}^3$

Year	$\lambda_{\odot 1}$	$\text{ZHR}_{\text{outburst}}$	$S_{6.5\,\text{outburst}}$	$\lambda_{\odot 2}$	ZHF_{max}	$S_{6.5\,\text{max}}$
1988	139°.78±0°.03	86±4	97±16	140°.08±0°.04	106±22	94±14
1989	139°.56±0°.03	102±10	127±23	139°.80±0°.09	94±6	120±20
1990	139°.55±0°.05	75±10	45±35	140°.54±0°.2	81±61	66±5
1991	139°.55±0°.03	284±63	494±150	139°.94±0°.04	97±2	124±20
1992	139°.48±0°.02	220±22	257±60	140°.13±0°.2	84±34	96±15
1993	139°.53±0°.01	264±17	242±62	139°.91±0°.04	86±2	79±44
1994	139°.59±0°.01	238±17	151±28	139°.84±0°.04	86±2	69±12
1988–1994	—	—	—	139°.96±0°.05	86±1	96±16

Wu and Williams (1995). Local maxima may simply be manifestations of groups of meteoroids with common ejection origin sharing similar values of nodal longitude and semi-major axis and thus being more numerous in one year as compared to others. This sharp variation in the flux would be a direct result of a sharp peak in the distribution of semi-major axes within such a meteoroid sub-population. Such groups may be a source for variations in the population index r during annual returns. A superposition of unevenly distributed data from the seven returns may keep some local features appearing in one or another r-profile.

In contrast, the main maximum shows a generally stable peak flux. Indeed, the peak spatial number densities from 1988 to 1994 associated with the main maximum vary from the average value $S_{6.5\,\text{max}}$ of 96 ± 16 by less than 30%. This result is in contradiction to past visual results which suggest large variations in $S_{6.5\,\text{max}}$. Zvolánková (1984) and Lindblad (1986) report variations of more than a factor of two in peak rates from visual observations made between the years 1944–1953 and 1953–1981, respectively. We suggest that these apparent variations are the result of biased sampling in these past visual observations resulting from uneven observer coverage.

The changes in $S_{6.5}$ associated with both maxima are given in Table 2. The average value for $S_{6.5\text{max}}$ of $96 \pm 16 \times 10^9$ and $11 \pm 2 \times 10^9\,\text{km}^3$ for $S_{3.5\text{max}}$, is in close agreement with the results of Kaiser *et al.* (1966) and Andreev *et al.* (1987) who, from radar observations, derive an average $S_{6.5\text{max}}$ of $1.3 \pm 0.2 \times 10^2 \times 10^9\,\text{km}^3$ and an $S_{3.5\text{max}}$ of $14 \times 10^9\,\text{km}^3$, respectively. Both radar observations were made at low frequency and thus should be relatively free of initial-train radius effects.

There are variations in the profiles of the population index of the stream (Fig. 9). There is an obvious asymmetry in particle makeup in the day leading to the main maximum when r is consistently low as compared to after the main maximum when r shows a significant increase. The average value of r for the remainder of the profile, both before and after the maxima, is remarkably constant near 2.1 with a general decrease from the beginning to $\lambda_\odot = 139°.35$ and a similar increase after $\lambda_\odot = 140°.10$ (Table 3). Two pronounced maxima in r are also evident near the time of the activity maxima. The first maxima in r occurs at $\lambda_\odot = 139°.56 \pm 0°.07$ and the second at $\lambda_\odot = 139°.88 \pm 0°.06$. The number of Perseid meteor magnitude estimates listed in Table 3 indicate that these features are statistically significant. These locations are potentially linked to the different evolutionary components of the stream. The first is probably related to the outburst component which is still present despite removal of the central portions of the outburst activity in each year. The young meteoroidal material associated with the latest return of 109P/Swift–Tuttle is enriched in smaller meteoroids as would be expected for recent ejecta. The main maximum is also enriched in fainter meteors indicating the presence of relatively young material.

A single local minimum in the population of small

Table 3. The population index, r, and the amount of data each r-value is based upon for the average profile 1988–1994 for the period $\lambda_\odot = 128°$–$144°$ (corresponding to July 31–August 18). The solar longitude is the mid-point of the interval over which averaging occurred

$\lambda_\odot$	r	Number of observers	Number of Perseids
128°.912	2.143±0.051	5	230
129°.401	2.120±0.037	9	383
130°.222	2.078±0.076	7	270
131°.749	2.003±0.037	12	454
132°.497	2.060±0.035	25	1029
133°.454	2.051±0.041	38	1858
134°.422	2.056±0.037	43	2150
135°.451	2.141±0.032	55	2859
136°.494	2.058±0.026	76	3819
137°.420	2.058±0.022	108	5963
138°.715	1.968±0.016	239	15,932
139°.045	1.930±0.018	172	11,931
139°.354	1.886±0.022	101	10,257
139°.362	1.913±0.021	118	11,369
139°.508	2.054±0.032	43	2806
139°.752	2.049±0.039	27	1870
139°.752	1.900±0.068	13	1140
139°.828	1.992±0.032	70	9001
139°.878	2.099±0.027	83	11,641
140°.011	2.055±0.034	61	5664
140°.107	1.873±0.031	76	5389
140°.224	1.987±0.024	117	9660
140°.307	2.022±0.022	162	15,257
140°.370	2.049±0.029	96	9638
140°.844	2.097±0.015	210	18,282
141°.021	2.104±0.013	252	21,191
142°.193	2.122±0.026	64	4004
143°.083	2.156±0.046	24	1035
143°.834	2.187±0.074	6	192

meteoroids just before maximum has been previously noted by Mason and Sharp (1981). Andreev *et al.* (1987) found a local maximum in the proportion of small meteoroids at the time of maximum from radar data. It seems probable that the different ages of the outburst and core components of the stream are manifest not only in higher flux but also in differences in the meteoroids population relative to the background population and that recent ejections of fresh meteoroids have significantly different r-values as shown by these visual data.

The outburst component of the stream has only been recognized in visual observations over the last few years (cf. Roggemans, 1989), though Lindblad and Porubčan (1994) have shown that photographic Perseid activity dating back as far as the 1950s had an earlier peak near the present nodal longitude for 109P/Swift–Tuttle. Šimek and Pecina (1996) also detected the presence of the outburst peak as early as 1986 in Ondřejov radar data and suggest that the sub-maxima reported at $\lambda_\odot = 139°.5$ by Šimek (1987) in earlier radar data may also be a detection of the outburst component of the stream. This component has been widely associated with the return of 109P/Swift–Tuttle to perihelion in 1992 and is generally regarded as consisting of material only one or at most a few revolutions old (Wu and Williams, 1993; Williams and Wu, 1994; Jones and Brown, 1996).

The position of the outbursts given in Table 2 shows a drift from $\lambda_\odot = 139°.78$ in 1988 to $139°.48$ in 1992. This is the closest approach to the node of the parent comet 109P/Swift–Tuttle. The next peaks shift away from this position and occur later. This trend has continued through to at least 1996 (Rendtel and Arlt, 1996). The relative magnitude of the peaks are shown in Fig. 10a where the number densities at the outburst peak are given relative to $S_{6.5\,\max}$. Here a clear demarcation occurs, with activity being weak before 1991 and strong thereafter. This sudden change in the outburst component, rather than a gradual increase in flux as predicted by model calculations presuming all new activity to result from 1862 ejecta (Williams and Wu, 1994) suggests that meteoroids encountered before 1991 may have a different origin. On the basis of model calculations, Jones and Brown (1996) ascribe the material from 1988 to 1990 as being almost exclusively from the 1737 and 1610 passages of 109P/Swift–Tuttle, with meteoroids from the 1862 passage being first encountered in significant quantities in 1991.

The location of the visual maxima in these years is very similar to that reported from overdense radar observations. Watanabe *et al.* (1992) analysed the 1991 Perseid return with the Kyoto MU-radar and determined the time of peak for the outburst component to be $\lambda_\odot = 139°.6$, in good agreement with the visual results. They also found that the outburst peak flux was 3.4 ± 0.8 times that of the main maximum. This result was valid for meteors in the magnitude range $0 > M_v > +3$ which is very similar to the ratio of spatial number densities we found between the outburst peak and the core maximum in 1991 of 3.2 in the same magnitude range (Fig. 10a). For comparison, Šimek and Pecina (1996) used the Ondřejov radar and found the maximum to be located at $\lambda_\odot = 139°.58 \pm 0°.04$ in the interval 1986–1994.

The particle composition of the outburst component of the stream is shown in Fig. 10b relative to the main peak, where the ratio of the respective population indices have been plotted. Interestingly, the proportion of bright meteors during the outbursts is not substantially different from the main peak and thus the mass distribution of the outburst in all years, as measured by r, is not different from the population associated with the core component of the stream in contradiction to the conclusions of Watanabe *et al.* (1992). This result is consistent with the earlier observation of a maximum in the r-values near the time of both maxima.

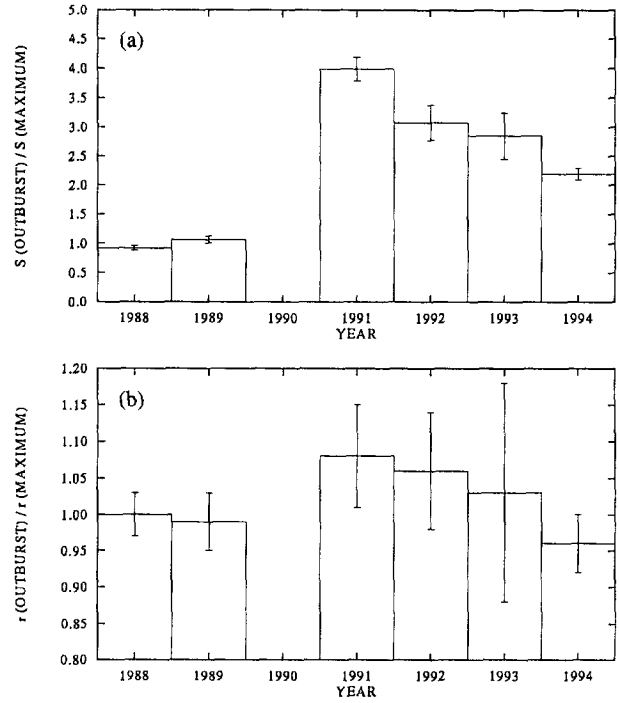

Fig. 10. The relative magnitude of the peak number density for the outburst component of the Perseids, $S_{6.5\,\text{outburst}}$, in units of $S_{6.5\,\max}$ for the given year (a). The change in relative particle composition between the outburst peak and main peak during 1988–1994 as denoted by the ratio of their respective population indices $r_{\text{outburst}}/r_{\max}$ (b). Data from 1990 has been omitted due to severe moonlight disturbance. The positions of the main peak have been taken from the ZHR values because of possible uncertainties in the profiles of the population index r and hence also in the number density S

4. Conclusions

The seven year study of the Perseid stream presented here makes it clear that visual meteor observations provide a useful diagnostic of stream activity. The correspondence between radar data and the visual data show the utility of both and the complementary nature of these two observational forms in meteor astronomy. The general validity of the reduction methods presented here for visual observations has been verified through early detection in 1988 of new material associated with the impending return of 109P/Swift–Tuttle (Roggemans, 1989). This is the first time that visual data has successfully "detected" the return of a comet through subtle variations in shower activity profiles before the comet was actually recovered.

From the flux data and particle population presented

here for the Perseid stream, several outstanding features of the stream must be explained by any successful Perseid model.

1. The asymmetry in the background Perseids and the symmetry in the core population as defined by the locations of the 1/4-width ($2^\circ.58 \pm 0^\circ.07$ before maximum and $2^\circ.35 \pm 0^\circ.07$ after maximum) and the 1/2-width ($1^\circ.06 \pm 0^\circ.07$ before maximum and $1^\circ.04 \pm 0^\circ.07$ after maximum) positions.
2. The location and magnitude of the outburst maxima for each year given in Table 2.
3. The location and magnitude of the mean activity maximum associated with the core population at $\lambda_\odot = 139^\circ.96 \pm 0^\circ.05$ and with $S_{6.5\max} = 96 \pm 16 \times 10^9\,\mathrm{km}^{-3}$.
4. The change in particle composition across the stream, particularly in the region near the maxima in r at $\lambda_\odot = 139^\circ.55 \pm 0^\circ.07$ (uncertain, see Section 3) and $\lambda_\odot = 139^\circ.88 \pm 0^\circ.06$.
5. The apparent similarity between the meteoroid populations associated with the outburst and core population.
6. The broad shoulder in flux after the core maximum.
7. The differing slopes in the branches of the outburst profile and the asymmetry in these profiles.
8. The origins of the background, outburst and core populations.

Other characteristics which are not conclusively discerned in these data, such as the possible presence of a sub-maximum near $\lambda_\odot = 140^\circ.2$–$140^\circ.3$ or at $\lambda_\odot = 140^\circ.5$ and the existence of ephemeral sub-maxima at various locations after the core maximum in different years, need further observational confirmation applying visual, photographic and video data from several locations.

In conclusion, the Perseid meteoroid stream is highly dynamic and rich in structure. The complexities of the Perseids can only be understood in the context of a complete numerical model of the stream and must explain features detected through observations such as those found here.

Acknowledgements. The authors are deeply indebted to all observers who contributed their observations to this study. Without their dedication this work would not have been possible. P.B. wishes to thank the Natural Sciences and Engineering Research Council for funding support. Discussions with J. Jones, R. Koschack and K. Yau helped to improve the paper.

References

Ahnert-Rohlfs, E. (1952) On the structure and the origin of the Perseid meteoroid stream. *Veröffentlichungen der Sternwarte Sonneberg* **2,** 5–38 (in German).

Andreev, G. V., Rubtsov, L. N. and Tarasova, N. V. (1987) On the spatial structure of the Perseids meteor stream. In *First GLOBMET Symposium*, ed. R. G. Roper, p. 339. ICSU-SCOSTEP, Urbana, Illinois.

Brown, P. and Rendtel, J. (1996) The Perseid meteoroid stream: characterization of recent activity from visual observations. *Icarus* **124,** 400–417.

Harris, N. W., Yau, K. C. C. and Hughes, D. W. (1995) The true extent of the nodal distribution of the Perseid meteoroid stream. *MNRAS* **273,** 999–1015.

Hasegawa, I. (1993) Historical records of meteor showers. In *Meteoroids and their Parent Bodies*, eds J. Štohl and I. P. Williams, p. 209. Astronomical Inst., Slovak Acad. Sci., Bratislava.

Jones, J. and Brown, P. (1996) Modelling the orbital evolution of the Perseid meteoroids. In *Proceedings of IAU Colloquium 150: Physics, Chemistry and Dynamics of Interplanetary Dust*, eds B. A. S. Gustafson and M. S. Hanner, pp. 105–109. Astronomical Society of the Pacific.

Kaiser, T. R., Poole, L. M. G. and Webster, A. R. (1966) Radio-echo observations of the major night-time streams. I. Perseids. *MNRAS* **132,** 224–237.

Koschack, R. (1995) Analyses and calculations. In *Handbook for Visual Meteor Observers*, eds J. Rendtel, R. Arlt and A. McBeath, pp. 280–289. IMO, Potsdam.

Koschack, R. and Hawkes, R. L. (1995) Observing instructions for major meteor showers. In *Handbook for Visual Meteor Observers*, eds J. Rendtel, R. Arlt and A. McBeath, pp. 42–74. IMO, Potsdam.

Koschack, R. and Rendtel, J. (1988) Number density in meteor streams. *WGN, The Journal of the IMO* **16,** 149–157.

Koschack, R. and Rendtel, J. (1990a) Determination of spatial number density and mass index from visual meteor observations (I). *WGN, The Journal of the IMO* **18,** 44–59.

Koschack, R. and Rendtel, J. (1990b) Determination of spatial number density and mass index from visual meteor observations (II). *WGN, The Journal of the IMO* **18,** 119–141.

Koschack, R. and Roggemans, P. (1991) The 1989 Perseid meteor stream. *WGN, The Journal of the IMO* **19,** 87–99.

Koschack, R., Arlt, R. and Rendtel, J. (1993) Global analysis of the 1991 and 1992 Perseids. *WGN, The Journal of the IMO* **21,** 152–168.

Kresáková, M. (1966) The magnitude distribution of meteors in meteor streams. *Contr. Skalnaté Pleso* **3,** 75–109.

Kronk, G. W. (1988) *Meteor Showers: A Descriptive Catalog.* Enslow, New Jersey.

Lindblad, B. A. (1986) Structure and activity of the Perseid meteor stream from visual observations 1953–1981. In *Asteroids, Comets, Meteors II*, eds C.-I. Lagerkvist, B. A. Lindblad, H. Lundstedt and H. Rickman, p. 531. Reprocentralen, Uppsala.

Lindblad, B. A. and Porubčan, V. (1994) The activity and orbit of the Perseid meteor stream. *Planet. Space Sci.* **42,** 117–122.

Lindblad, B. A. and Šimek, M. (1986) The activity curve of the Perseid meteor stream from Onsala radar observations 1953–78. In *Asteroids, Comets, Meteors II*, eds C.-I. Lagerkvist, B. A. Lindblad, H. Lundstedt and H. Rickman, p. 537. Reprocentralen, Uppsala.

Lovell, A. C. B. (1954) *Meteor Astronomy.* Oxford University Press, London.

Marsden, B. G. (1973) The next return of the comet of the Perseid meteors. *Astron. J.* **78,** 654–662.

Marsden, B. G., Williams, G. V., Kronk, G. W. and Waddington, W. G. (1993) Update on comet Swift–Tuttle. *Icarus* **105,** 420–426.

Mason, J. W. and Sharp, I. (1981) The Perseid meteor stream in 1980. *JBAA* **91,** 368–390.

Rendtel, J. and Arlt, R. (1996) Perseids 1995 and 1996—an analysis of global data. *WGN, The Journal of the IMO* **24,** 141–147.

Rendtel, J., Brown, P. and Molau, S. (1996) The 1995 outburst and possible origin of the α-Monocerotid meteoroid stream. *MNRAS* **279,** L31–L36.

Roggemans, P. (1989) The Perseid meteor stream in 1988: a double maximum! *WGN, The Journal of the IMO* **17,** 127–137.

Šimek, M. (1987) Perseid meteor stream mean profile from radar observations in Czechoslovakia. *BAC* **38,** 1–6.

Šimek, M. and McIntosh, B. A. (1986) Perseid meteor stream mean flux curve from radar observations. *BAC* **37,** 146–155.

Šimek, M. and Pecina, P. (1996) Activity of the new filament of

the Perseid meteor stream. In *Proceedings of IAU Colloquium* 150: *Physics, Chemistry and Dynamics of Interplanetary Dust*, eds B. A. S. Gustafson and M. S. Hanner, pp. 109–113. Astronomical Society of the Pacific.

Verniani, F. (1973) An analysis of the physical parameters of 5759 faint radio meteors. *J. Geophys. Res.* **78,** 8429–8462.

Watanabe, J.-I., Nakamura, T., Tsutsumi, M. and Tsuda, T. (1992) Radar observations of the strong activity of a Perseid meteor shower in 1991. *PASJ* **44,** 677–685.

Williams, I. P. and Wu, Z. (1994) The current Perseid meteor shower. *MNRAS* **269,** 524–528.

Wu, Z. and Williams, I. P. (1993) The Perseid meteor shower at the current time. *MNRAS* **264,** 980–990.

Wu, Z. and Williams, I. P. (1995) Gaps in the semimajor axes of the Perseid meteors. *MNRAS* **276,** 1017–1023.

Yau, K., Yeomans, D. and Weissman, P. (1994) The past and future motion of comet P/Swift–Tuttle. *MNRAS* **266,** 303–316.

Zvolánková, V. (1984) Changes in the activity of the Perseid meteor shower 1944–1953. *Contr. Obs. Skalnaté Pleso* **12,** 45–75.